LANL Report LA-UR-01-3161

Los Alamos
NATIONAL LABORATORY

memorandum

LANSCE Division

Group Lansce-1

To/MS: Distribution
From/MS: T. Tajima, LANSCE-1, MS H817 田島 健
Phone/Fax: 7-6559/5-2904
E-mail: tajima@lanl.gov
Symbol: LANSCE-1:01-048
Date: May 2, 2001

Subject: RESULTS OF LOW TEMPARETURE TESTS ON ANL SPOKE CAVITY (340 MHz, beta=0.291)

Contributors: A. Shapiro, M. Madrid, F. Krawczyk, R. Gentzlinger, D. Montoya, B. Haynes and R. Edwards

Abstract

To predict achievable Q_0 and accelerating field E_{acc}, we applied to ANL cavity our present techniques for cavity testing that have been used for APT cavities. We etched the cavity 100 microns with BCP (Buffered Chemical Polish) followed by HPR (High Pressure Rinse) with 1000 psi DI water in our clean room. Before the measurement, we baked the cavity at 150 °C (spoke) and at 80 °C (at indium flanges). Test results showed low-field Q_0 at Eacc ~1 MeV/m of 2.3E9 (4 K) and 8.6E9 (2 K). The maximum E_{acc} were 12.5 MeV/m (4 K) and 12.3 MeV/m (2 K). These maximum accelerating fields were obtained after ~5 minutes of helium processing. This memorandum describes the detail of the tests.

Distribution:

K.C. Chan, AAA-TPO, MS H816 R. Edwards, MST-6, MS G770 R. Garnett, LANSCE-1, MS H817 R. Gentzlinger, ESA-DE, MS H821 W. B. Haynes, LANSCE-9, MS H851 A. Jason, LANSCE-1, MS H817 P. Kelley, LANSCE-1, MS H817 F. Krawczyk, LANSCE-1, MS H817 J. Kuzminski, AAA-TPO, MS H816 R. LaFave, LANSCE-1, MS H817 M. Madrid, AAA-TPO, MS H816 D.I. Montoya, ESA-DE, MS H821 P. Roybal, LANSCE-1, MS H817 E. Schmierer, ESA-DE, MS H821 D. Schrage, LANSCE-1, MS H817	S. Schriber, ALDSSR, MS H817 A. Shapiro, LANSCE-1, MS H817 R. Sheffield, AAA-TPO, MS H816 R. Valdiviez, LANSCE-1, MS H817 T. Wangler, LANSCE-1, MS H817 J. Waynert, ESA-EPE, MS J580 R. Wood, LANSCE-1, MS H817 AAA-TPO Reading File, MS H816 LANSCE-1 Reading File, MS H817 Ken Shepard, Argonne National Lab, Physics Division-Bldg. 203, Argonne, IL 60439 Mike Kelly, Argonne National Lab, Physics Division-Bldg. 203, Argonne, IL 60439

1. Introduction

The detail of the cavity was described elsewhere [1]. This cavity was tested at ANL before it was loaned to LANL. Figure 1 shows the results. As one can see, this cavity has suffered field emission starting around 3.5 MeV/m. The difference between ANL and LANL at the time of this experiment is that we have a better clean room and HPR facility to clean and handle the cavity. Our objectives of testing the ANL cavity at low temperature were: (1) identify the difference from elliptical cavities in terms of the cavity behavior such as multipacting barriers and (2) know achievable Q_0, E_{acc} and residual resistance with our present procedure that has been applied to APT elliptical cavities such as BCP, HPR, assembly and processing techniques such as RF processing and helium processing.

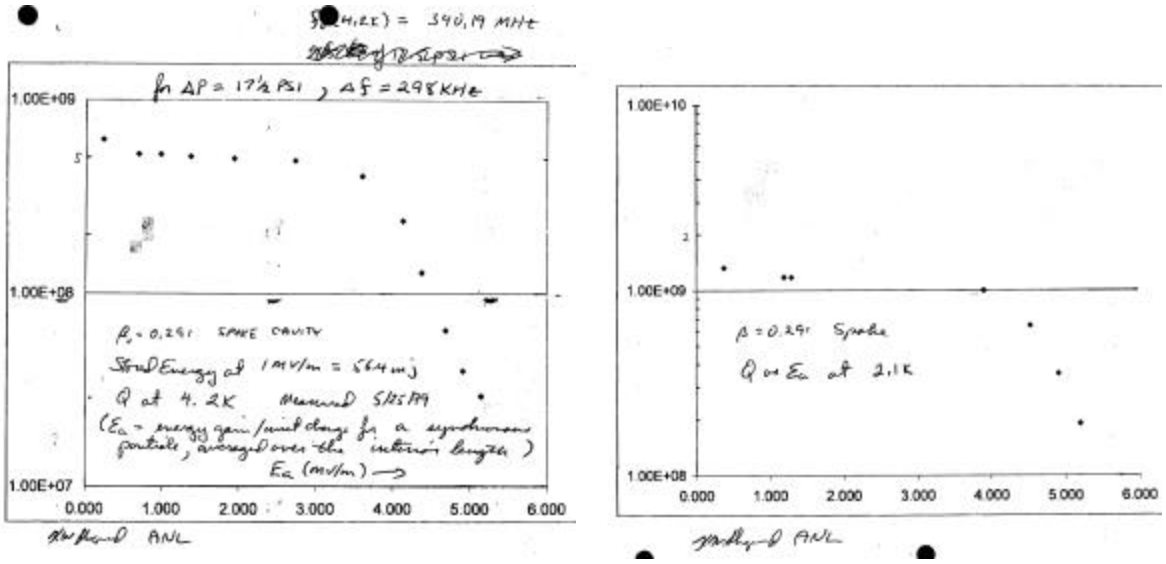

Fig. 1: Q_0 vs. E_{acc} obtained at ANL at 4.2 K (left) and at 2.1 K (right) [2].

Table 1: Parameters calculated with MAFIA [4].

Effective cavity length	0.1765 m
ZT^2/Q	295.4 Ω
Geometrical factor, G	70.7 Ω
E_{pk}/E_{acc}	3.18
H_{pk}/E_{acc}	85 Gauss/MV/m

2. Preparation and testing

2.1. BCP (Buffered Chemical Polishing)

The BCP facility at MST-6 was modified to accommodate the ANL cavity. The change to be noted is the sealing of flanges. We changed the o-rings from Viton to Teflon-encapsulated Viton as being used at JLAB to avoid contamination of the cavity with particles that may come off from the o-rings. Figure 2 shows the ANL cavity plumbed with PVDF pipes to the containers of chemicals. (See more pictures in Appendix 9.1) Figure 3 shows the etching rate measured with three samples. All

the chemicals, i. e., nitric, hydrofluoric and phosphoric acid, were renewed before this BCP. The BCP solution consists of these chemicals in a volumetric ratio of 1:1:2. The BCP solution is contained in the bottom tank and is pumped up to the cavity and goes into a heat exchanger, then goes back to the bottom tank. The estimated flow rate of the circulating BCP solution was ~10 gallons/min. The bath temperature and cavity outside temperature during BCP were 7.2-11.4 °C and 15-17 °C, respectively. The etching rate calculated from Fig. 3 is 0.5 μm/min. As compared to previous 0.3 μm/min, the etching rate increased probably due to this renewal of the chemicals. After the BCP, we filled the cavity with DI water overnight after coarse rinsing. This process was added because it may have caused the improvement of Q_0 of LANL elliptical cavity in the last test. (LANL cavity showed the best Q_0 of 3.6×10^{10} at 2 K.)

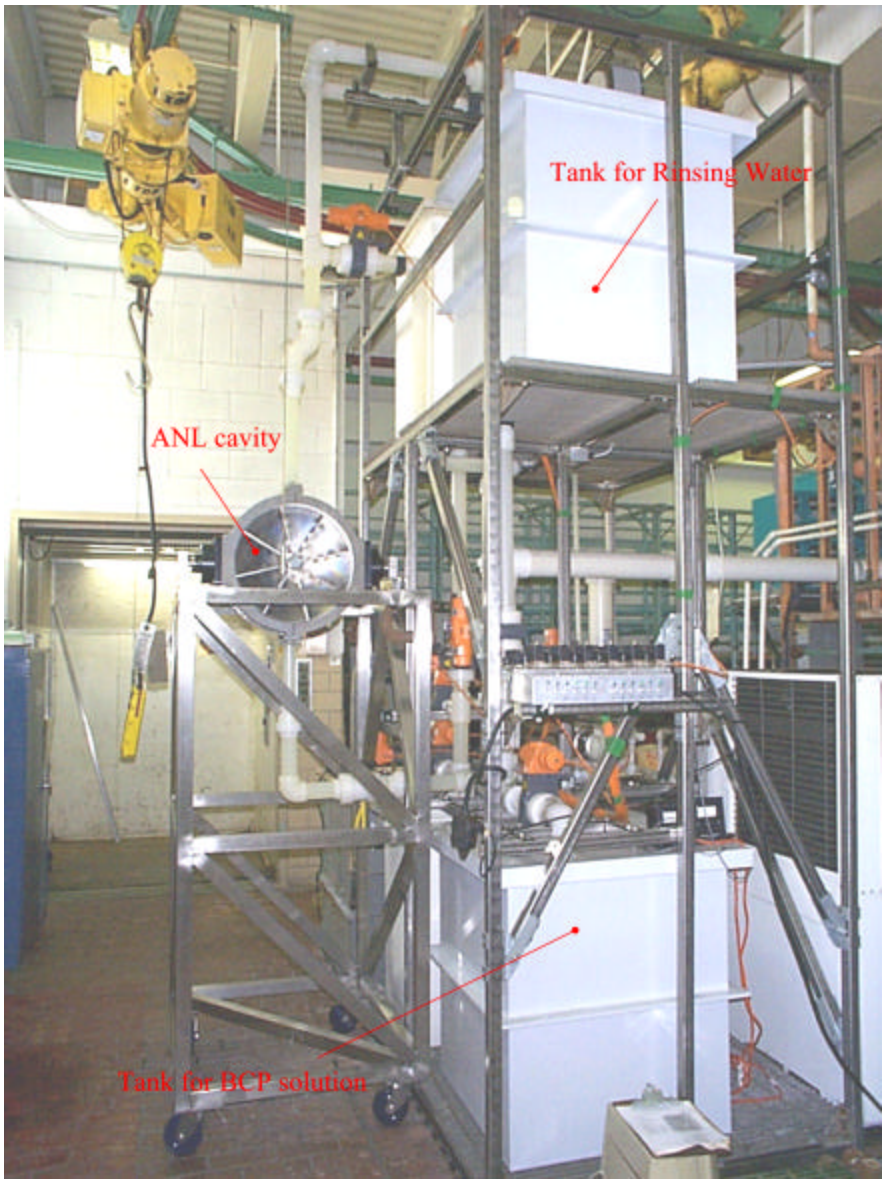

Fig. 2: ANL cavity set for BCP at MST-6.

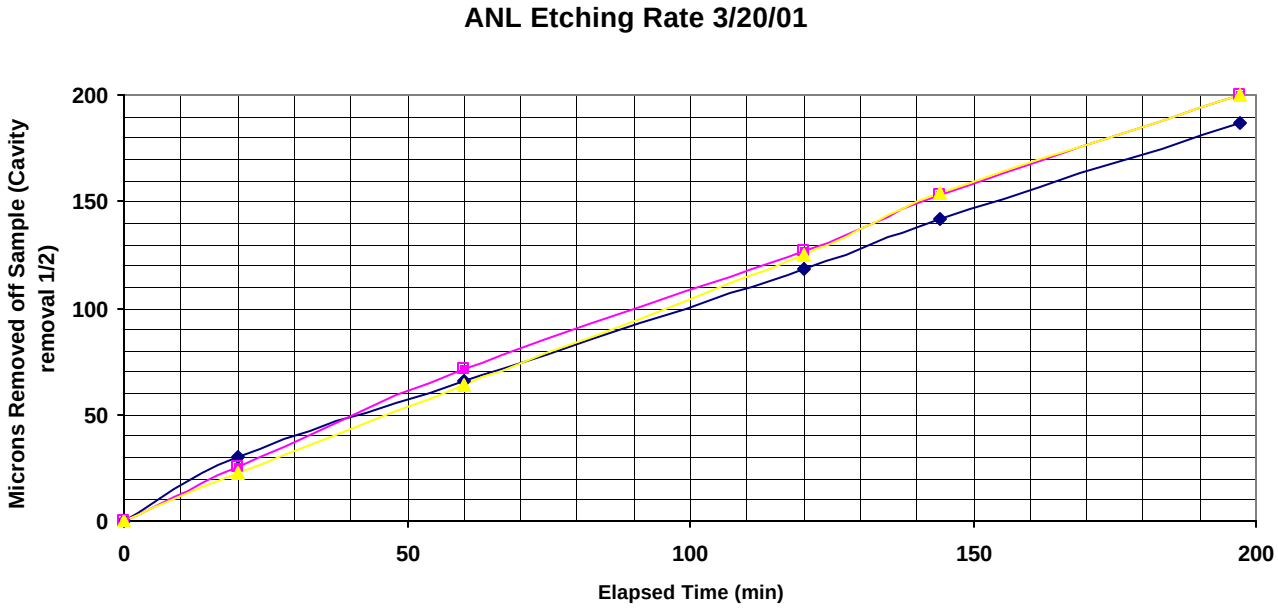

Fig. 3: Reduction of thickness of three Nb samples during BCP. The etched amount is half of this value.

2.2. HPR (High Pressure Rinsing)

Since the shape of ANL cavity is very different from that of elliptical cavities and more complicated, the design of the HPR nozzle and the procedure were elaborated. The diameter of nozzle holes were identical with that for APT cavities, but angles of the water jet were changed so that at least one of the jets hit every surface and all the surfaces were cleaned thoroughly. Figure 4 shows the design of the nozzle. Total of 15 holes of 0.018-inch diameter were drilled on a 0.5-inch diameter and 0.15-inch thick 316 stainless steel pipe. Figure 5 shows the force of the water coming out of each hole, which was calculated from the flow rate and water velocity assuming that water density is 1 g/cm^3. The maximum pump pressure was 1150 psi. The total flow rate, flow rate from each hole and water velocity at a pump pressure of 1000 psi were 7.62 liters/min, 8.5 cm^3/sec and ~52 m/s, respectively. Table 2 summarizes the parameters we used for the HPR together with these data.

HPR was performed at a pump pressure of 1000 psi in four steps. Figure 6 shows schematics to illustrate the steps. The left figure shows the cavity position during the first two steps, i.e., the nozzle goes up and down through the axial ports. The second step is to flip over the cavity and do the same HPR. The right figure shows the cavity position during the third and fourth steps. The nozzle goes through the radial port on the top, but it stops halfway because there is a spoke in the way. The nozzle goes up and down between the top port and the spoke for a few times. After this step, the cavity is flipped over and the same cleaning is performed. Though we planned to move the cavity horizontally to clean the spoke surface that could not be covered by the jet, it was not necessary because the nozzle was shaking horizontally by about 1/2 inch. Also, we did not rock/tilt the cavity to facilitate the draining through the bottom port because the amount of water that was draining

through the bottom port seemed to be large enough to form a strong natural flow to rinse off the chemical residues and particles through the bottom port. Figure 7 shows a photograph during the last step. The large diameter pipe taped on top of the top port is a cover to prevent splash when the water jet hits the top port.

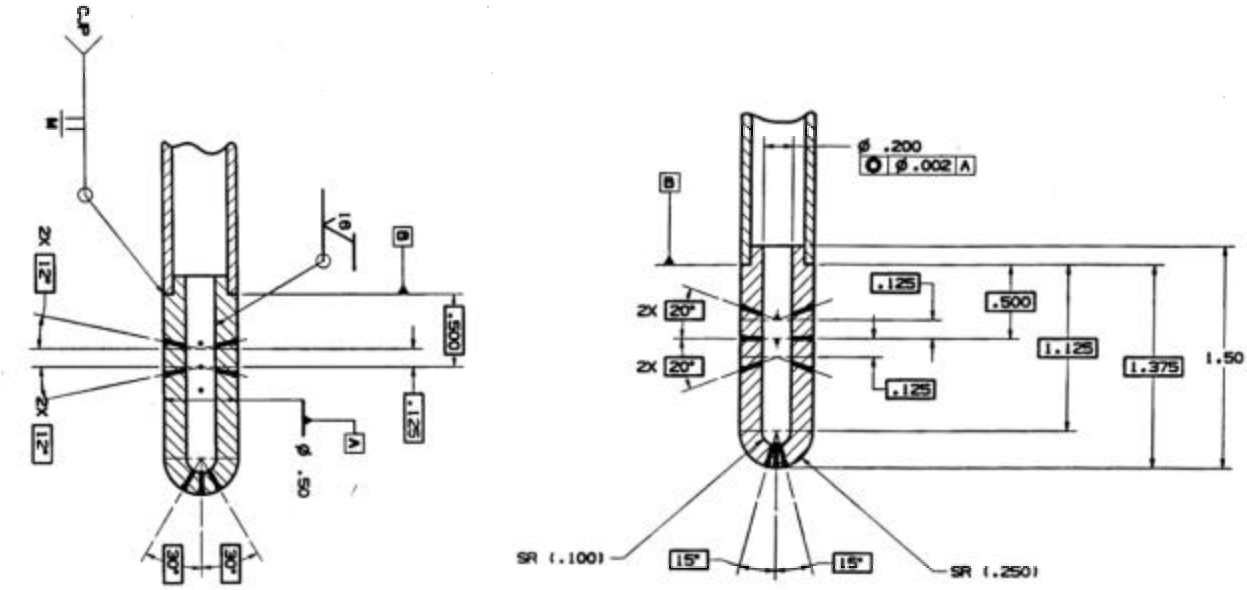

Fig. 4: Cross sections of HPR nozzle. Right drawing is 90° rotated compared to the left drawing.

Table 2: Parameters for HPR.

DI water pressure	1000 psi
Total flow rate	7.62 liters/min.
Flow rate through each hole	8.5 cm^3/sec
Table rotation speed	26 RPM
Nozzle up/down speed	~2.4 in./min.
Number of sweeps per step	10 sweeps (40 sweeps for 4 steps)
Total rinsing time	~2 hours

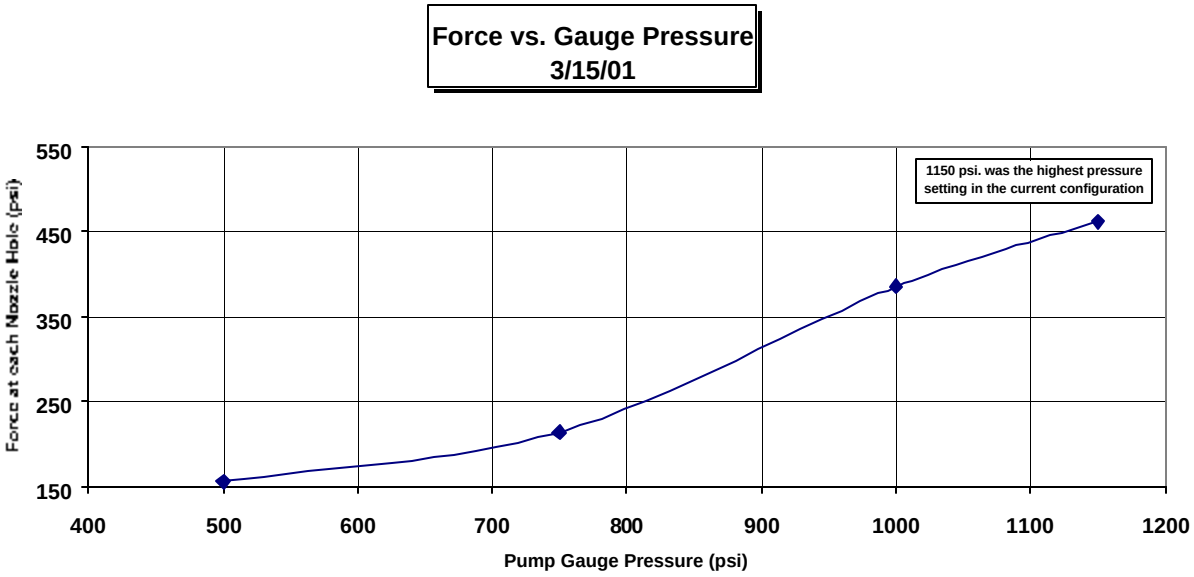

Fig. 5: Force at each nozzle hole as a function of pump gauge pressure.

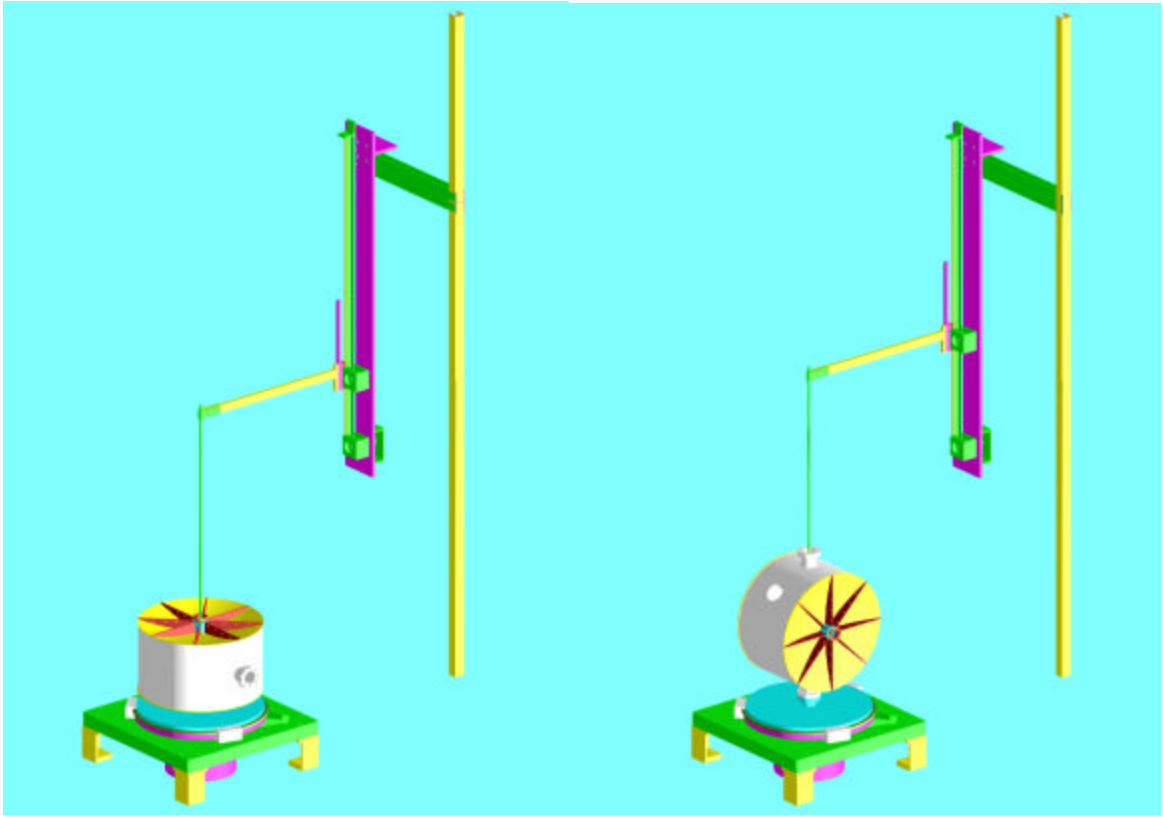

Fig. 6: Schematics to illustrate the cavity positions during HPR

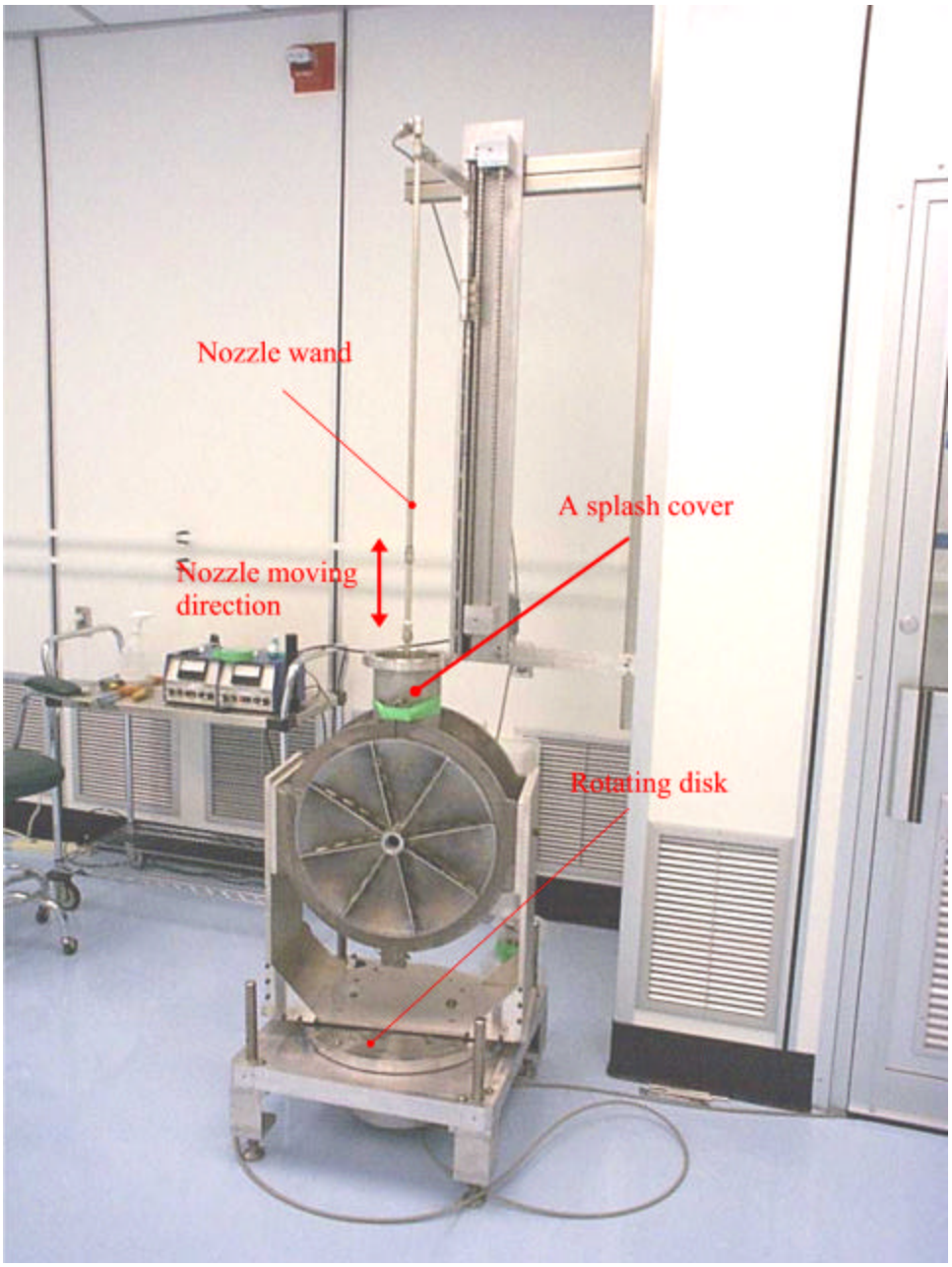

Fig. 7: A photograph during the HPR in the class-100 clean room.

2.3. Assembly

After HPR, we installed an input coupler and a pick-up antenna on the axial ports, and a vacuum valve and a blank flange on the radial ports. Since all the flanges were made for indium seals as opposed to the conflat flanges that we normally use for APT cavities, we made the adapter flanges that match the conflat flanges used for existing coupler driving mechanism and other ports. Figure 8 shows the cross sections of the input coupler port and pick-up port when assembled. The input coupler travels horizontally 2 inches with a scissor-hand-type moving mechanism so that enough

coupling at both 4 K and 2 K can be obtained. The input coupler is made of thin-wall hollow aluminum pipe so that no support is necessary between the end connector and the tip of the coupler.

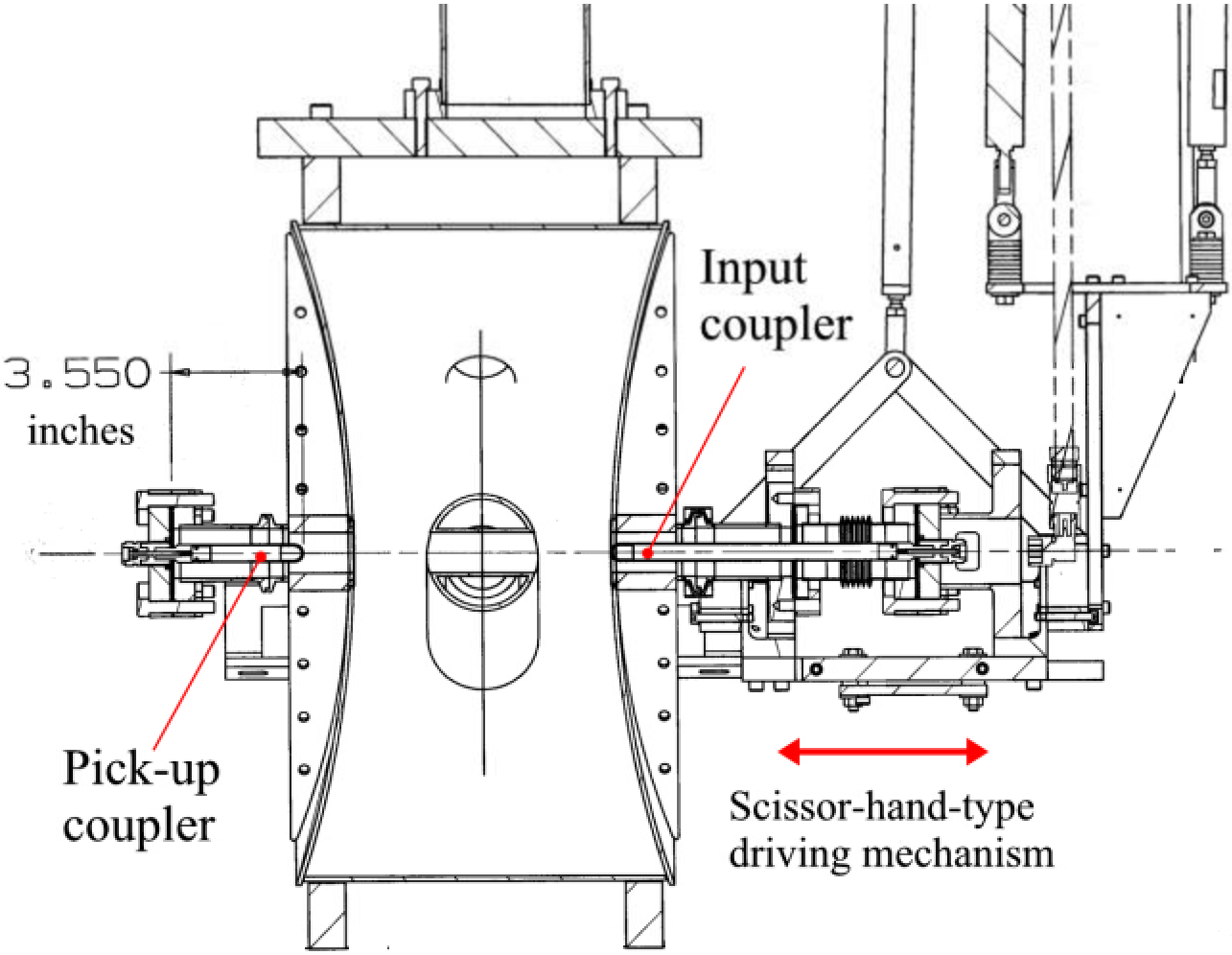

Fig. 8: Cross section of the input and pick-up couplers and associated flanges.

Figure 9 is a photograph showing the way indium wire was set on the flange. A polyethylene disk that fits in the flange was made to center the wire. This method has been used at KEK since TRISTAN era. Figure 10 is another photograph taken when assembling the input coupler with a bellows was assembled.

Figures 11 and 12 show a schematic when set on the insert and a photograph of the cavity actually set on the insert, respectively. The angle of the spoke from horizontal plane was measured to be 16 degrees. We tried to make this angle as much as possible to facilitate the natural helium flow in the spoke, but we could not move much due to the stiffness of the flexible vacuum line. On the other hand, this test could show that we can get up to 12.5 MeV/m even with this angle as will be shown later.

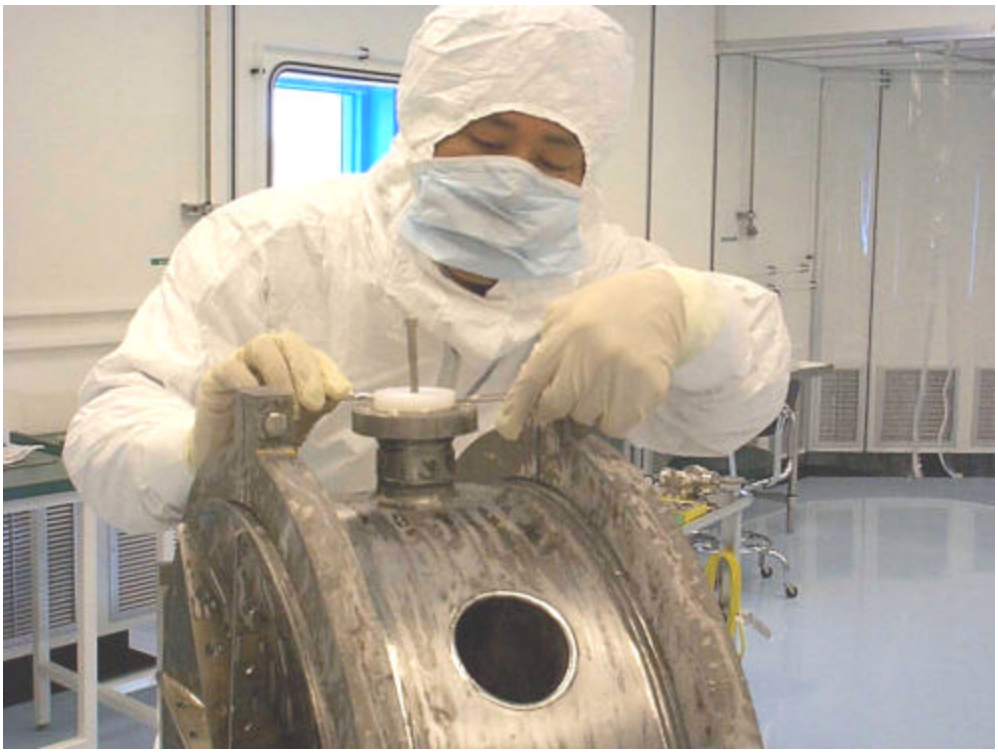

Fig. 9: Setting an indium wire (1 mm in diameter).

Fig. 10: Assembling the input coupler with bellows.

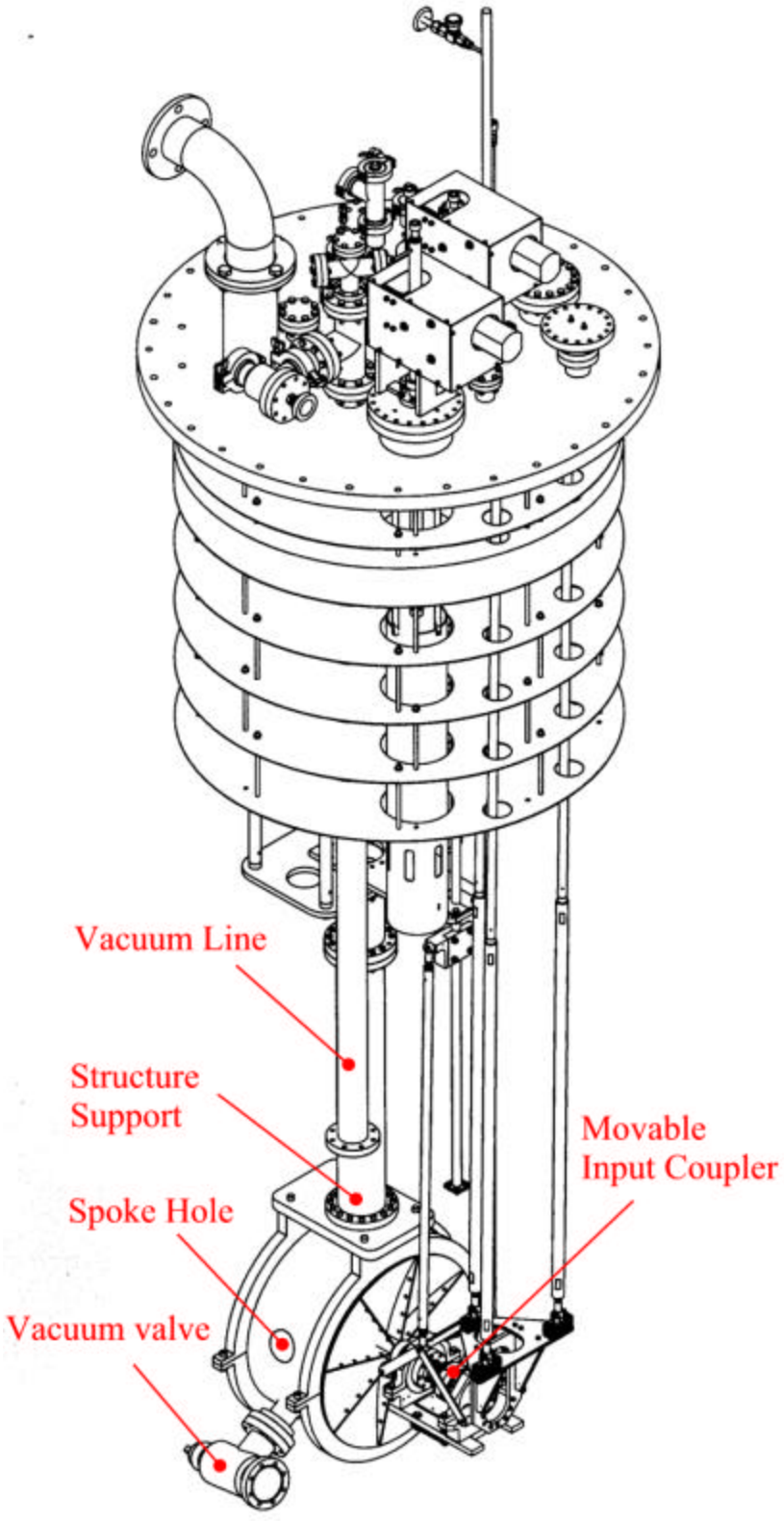

Fig. 11: A schematic of the ANL cavity set on the cryostat insert. The flexible vacuum line connecting the valve and straight line is not shown to show the cavity itself in more detail.

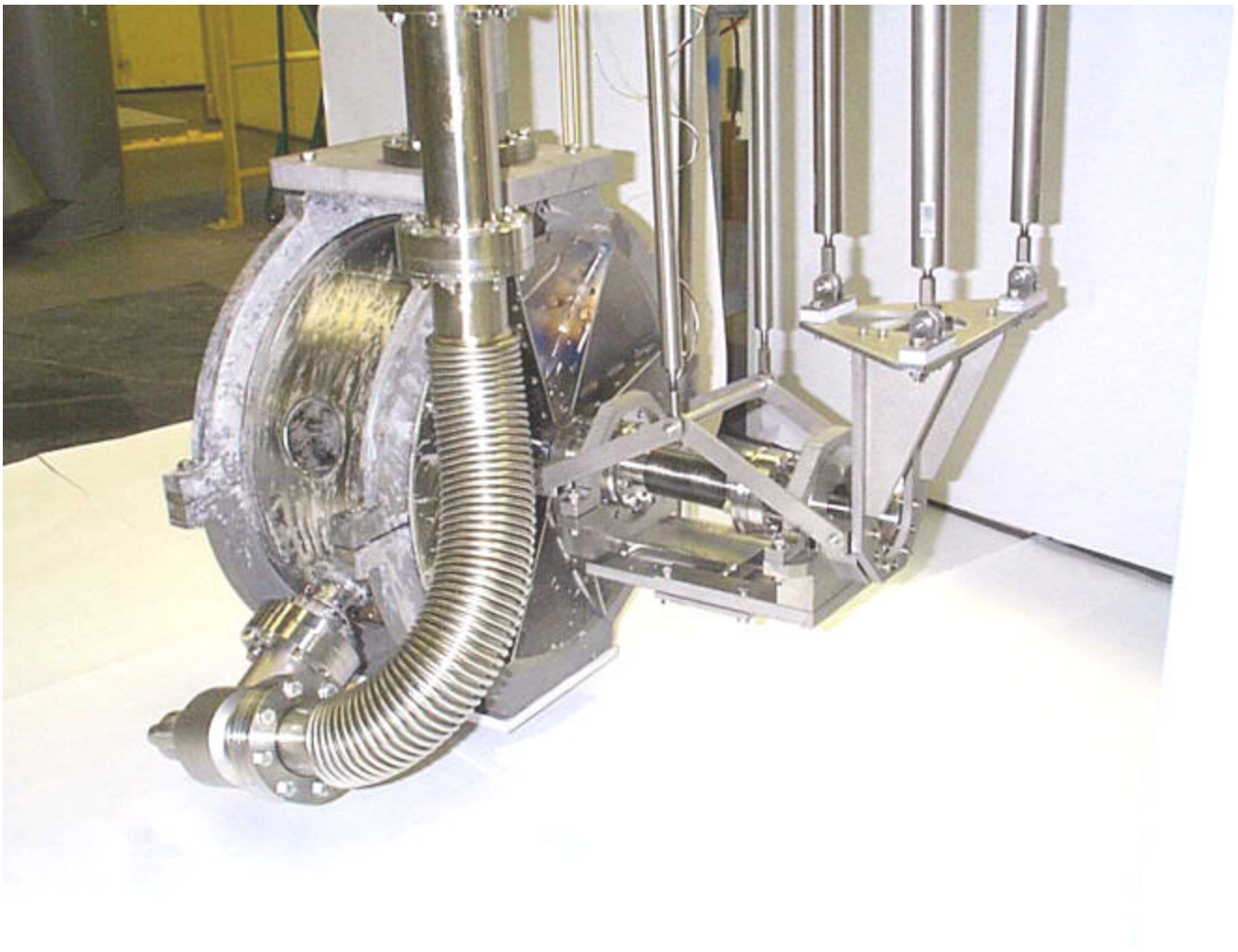

Fig. 12: A photograph of ANL cavity set on the insert of vertical cryostat.

2.4. Diagnostics

Outside temperatures and X-rays at interesting points on the spoke wall and on the sidewalls such as high magnetic and electric field region were monitored with Allen-Bradley resistors and PIN diodes, respectively. The high magnetic and electric field regions were determined with MAFIA calculations [3]. It showed that the highest magnetic field, i.e., highest RF loss, region is on the spoke and ~ 3.4 cm from the joint with outer cavity wall.

We made two aluminum cylinders on which a few strips of sensor-mounted Be/Cu spring are attached as shown in Fig. 13 (X-ray sensors are not shown). These cylinders were inserted in the spoke holes. At first, we planned to support these cylinders using some stiffening plates on the end walls, but we found it unnecessary since the cylinders hold them selves in the spoke holes as shown on the right photograph in Fig. 13. The bar attached to the cylinder was going to be used for this purpose.

On the end walls, we only attached X-ray sensors due to lack of preparation time for the temperature sensors. Eight PIN diodes are placed close to the beam hole at every 45 degrees apart on each end

wall. Figure 14 shows the sensor positions. "R" and "D" mean the resistor (temperature sensor) and the diode (X-ray sensor), respectively. The highest magnetic region corresponds to the resistors R11 – R14. The neighbor strips are 1 inch away from this.

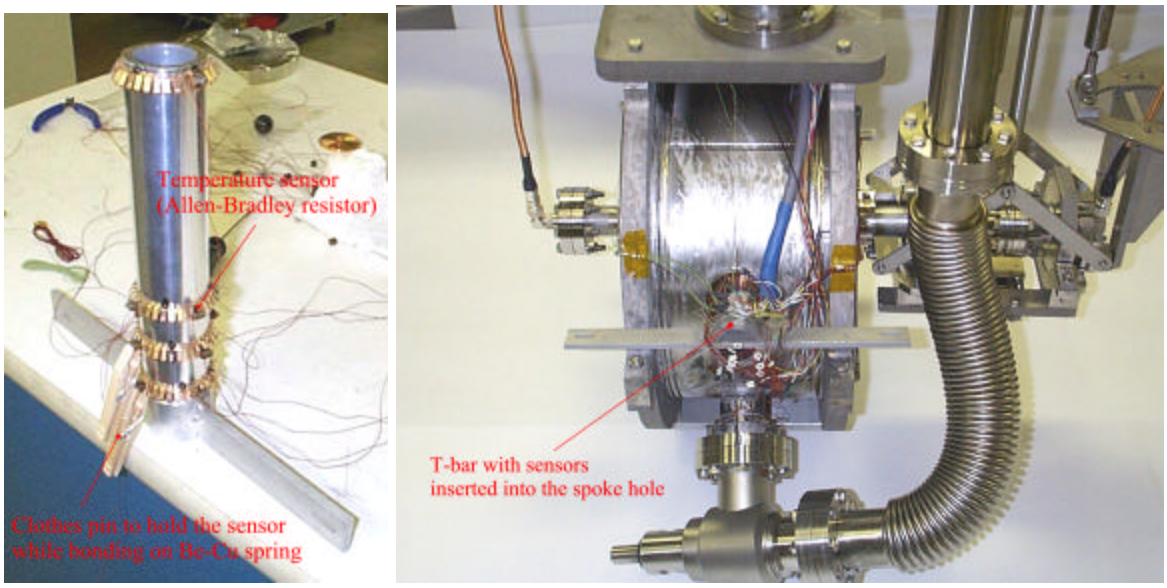

Fig. 13: Temperature sensors being bonded on Be/Cu spring (left) and the T-bar inserted in the spoke hole (right).

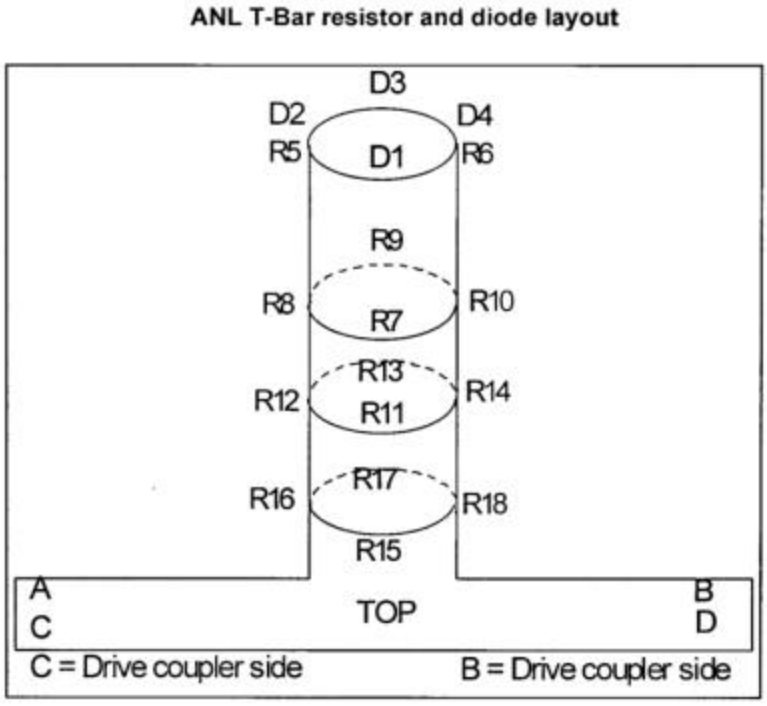

Fig. 14: Positions of the temperature sensors (resistors) and X-ray sensors (PIN diodes). "A" and "B" are written on one T-bar, and "C" and "D" are written on another T-bar.

In addition to these sensors, we had a radiation monitor and a NaI detector on the cryostat lid.

2.5. RF system

We modified our 700 MHz system being used for APT cavities. The components we changed are RF amplifier, RF filters. Also, a few phase shifters were added later during the test after having found that pre-existing phase shifter can change only about 90 degrees at 350 MHz and using the phase shifter over this range caused a lot of noise in the signal of the reflecting power. As for the amplifier, we ordered a 600 W RF amplifier that can operate at 200-1000 MHz, but the delivery was delayed and we could not use this amplifier. Instead, we borrowed a 200 W 350 MHz amplifier from LANSCE-5 [5].

2.6. Cool down

We pre-cooled the cryostat by filling the outer layer with liquid nitrogen. The cavity temperature after keeping the liquid nitrogen overnight was 268 K. About 600 liters of liquid helium was used to cover the cavity, which corresponds to 26.5 % of the bottom level sensor. To test at both 4 K and 2 K, liquid level of >50 % before pump down was necessary since we lost ~20 % during pumping and measurements. However, ~60 % would be preferable for processing and diagnosis of the cavity, which is estimated to be a total of 1140 liters of helium. In addition, though we can add some helium through J-T valve while pumping down, we tried not to do this to save time and helium.

2.7. RF tests

RF measurements were done in a very similar fashion with elliptical cavity tests. Since the parameters shown in Table 1 were different from the ones used for elliptical cavities, we changed those parameters in the LabView program. Except that, the measurements were the same as the ones with elliptical cavities.

3. Test results

Figure 15 shows Q_0 as a function of accelerating gradients (E_{acc}) in various conditions. The legends are shown in chronological order.

In the first 4 K measurement (solid triangles), the cavity showed field emission starting around 5 MeV/m and limited at 7.3 MeV/m with heavy electron loading and available RF power [6]. The next day, we pumped down the cryostat and performed the measurement at 2 K as well as taking low-field Q_0 data (~1 MeV/m) at various temperatures to calculate residual resistance. At 2 K, as shown in open circles in Fig. 15, low-field Q_0 increased to 8.5×10^9, but field emission started around the same field 5 MeV/m and Q_0 degraded reaching the same point as 4 K measurement. We kept the power at the maximum level for about one hour (this is called RF processing), then the maximum field gradually improved to 8.3 MeV/m as shown in x's in Fig. 15.

3.1. Helium processing

Compared to RF processing which uses the enhanced RF field at the emission site(s) to process the field emission, helium processing uses helium gas that is ionized with the field-emitted electrons. Due to much heavier mass of helium ions compared to electrons, this processing is often more effective in increasing maximum field than RF processing. A drawback of this processing is that a degradation of low-field Q_0 often occurs.

We switched ion pumps to 550 L/s turbo pump and fed helium gas through a cold trap (liquid nitrogen) to reach above 1.5×10^{-5} Torr. Then we controlled the pressure around 1.5×10^{-5} Torr by remotely opening/closing the turbo pump head valve at the console during the processing [7]. Though the real helium gas pressure in the cavity is not known since the pressure gauge is attached on the lid and it is not calibrated for helium ions, a pressure ~1.5×10^{-5} Torr on the lid seems to be the best condition for the processing, which is consistent with the past experience with 700-MHz APT 5-cell cavities.

Solid diamonds in Fig. 15 show the results after ~5 minutes of processing at 2 K. The maximum field increased to 12.3 MeV/m. In general, the processing time varies from one test to another, depending on the nature of the emission source(s) and its location(s). Normally, we do not continue more than 2 hours. This processing was one of the quickest ones in our experience. We already saw some improvement, i.e., increase of the transmitted power from the pick-up port soon after we started the processing and measurement simultaneously. Low-field Q_0, however, degraded by 3.2×10^9, which corresponds to an increase of surface resistance by 5 nΩ.

Solid squares show the result after warming up to 4 K. This was done to see if the effect of helium processing remains at 4 K. As one can see, the maximum field reached 12.5 MeV/m, which is almost the same as that at 2 K. Both at 2 K and 4 K, the field limitations were quenching. Low-field Q_0 degraded slightly by 0.1×10^9, which corresponds to an increase of the surface resistance by 2 nΩ.

Open diamonds show the result obtained after pumping down again to check the reproducibility of the result at 2 K. As one can see, the data overlapped with the previous 2 K data (solid diamonds) after helium processing, showing a good reproducibility.

3.2. Warm up to 30-70 K

Knobloch of Cornell Univ. says that the thermocurrents caused by the large radial temperature gradients at the normal conducting-superconducting boundary during thermal breakdown, create magnetic flux and these flux get trapped in reverting to superconducting state [13]. An increased surface resistance, i.e., degraded Q_0, results. He has observed that the increased surface resistance by breakdowns went back to the original value when he warmed up above transition temperature (9.22 K for niobium) and cooled down slowly [14]. Since thermal breakdowns occur during helium processing due to the bombardments of helium ions on the cavity surfaces, this theory may be applied to our case.

To confirm this, we transferred liquid helium back to a liquid helium dewar and warmed up the cavity to 30-70 K [8]. The stars of Fig. 15 show the result after cooling down again and pumping down to 2 K. As one can see, low-field Q_0 did not recover, indicating that some different

mechanism is responsible for this phenomenon. In addition, the maximum field degraded back to the value close to the one after RF processing before helium processing. We tried helium processing for about 10 minutes and confirmed that it can improve again as shown in crosses in Fig. 15, although we could not continue processing due to shortage of liquid helium.

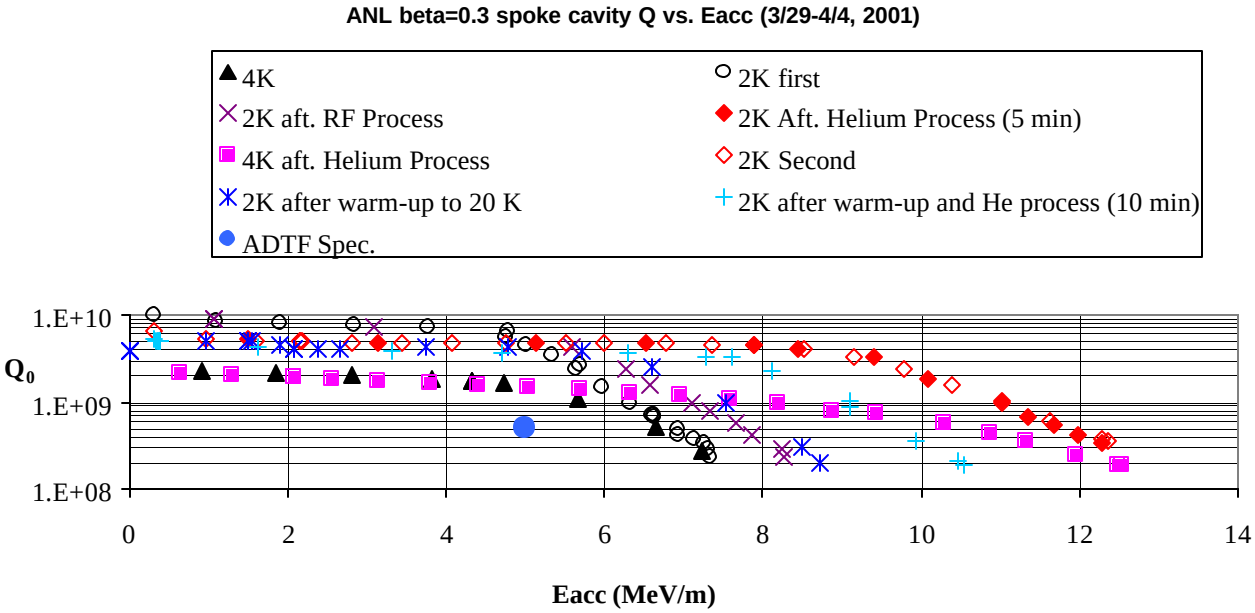

Fig. 15: Q_0 vs. accelerating field in various conditions.

3.3. Surface resistance and residual resistance

Though the data analyses have not been finished yet, a preliminary results show that the temperature at R5 increases more than the high magnetic field region, implying that the quench at 12.5 MeV/m occurred with the bombardment of electrons.

Surface resistance, R_s, can be calculated using Q_0 as R_s = (Geometrical factor)/Q_0, e.g., 70.7 Ω/Q_0 for the ANL cavity. Also, surface resistance is expressed theoretically as $R_s = R_{BCS}(f, T) + R_{res}$, where R_{BCS} is a function of frequency and temperature and called BCS resistance, and R_{res} is independent of these values and called residual resistance, which is affected by ambient magnetic field before cooling down or surface conditions of the cavity.

The formula for the surface resistance is written as follows [9].

$$R_S = A*1/T*f^2*\exp[-\Delta/kT] + R_{res} \quad , \tag{1}$$

where A is a constant dependent on the material parameters of the superconductor, such as the penetration depth, the coherence length, the Fermi velocity, and the mean free path. 2Δ is the energy gap of the superconductor, i.e., the energy needed to break the Cooper pairs. k is the Boltzmann constant.

Ref. [10] gives a practical formula for BCS resistance as follows.

$$R_{BCS} = 2\times10^{-4} * 1/T * \left(\frac{f[GHz]}{1.5}\right)\exp[-17.67 * 1/T] \quad (2)$$

Figure 16 shows low-field (~1 MeV/m) Q_0 as a function of cavity temperature. Using these data, surface resistances were calculated and are shown as a function of 1/T in Fig. 17. The solid line in Fig. 17 shows the fitting curve described in the insert of the plot. The residual resistance obtained from the fitting curve was 8.5 nΩ as shown in the insert. This value is the one before helium processing. As mentioned before, 2-5 nΩ of resistance was added to this after helium processing.

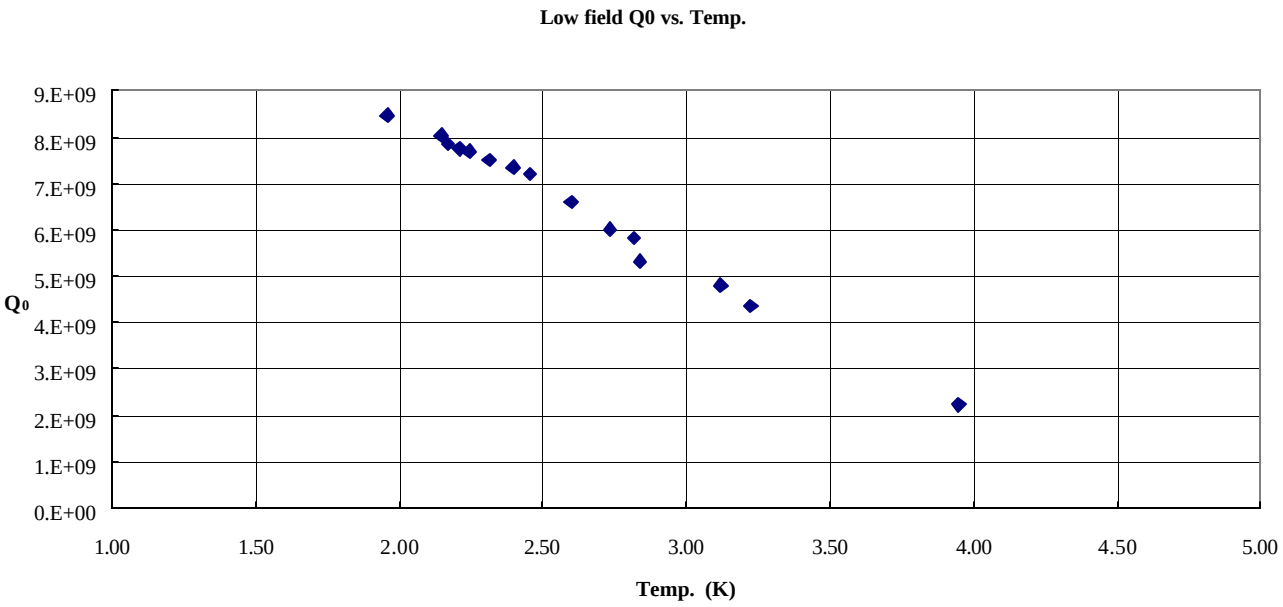

Fig. 16: Low-field Q_0 as a function of measurement temperature.

3.4. Diagnostics

3.4.1. Temperature

Though the data analyses have not been finished yet, a preliminary results show that the temperature at R5 increases more than the high magnetic field region, implying that the quench at 12.5 MeV/m occurred with the bombardment of electrons that hit the inside wall of R5.

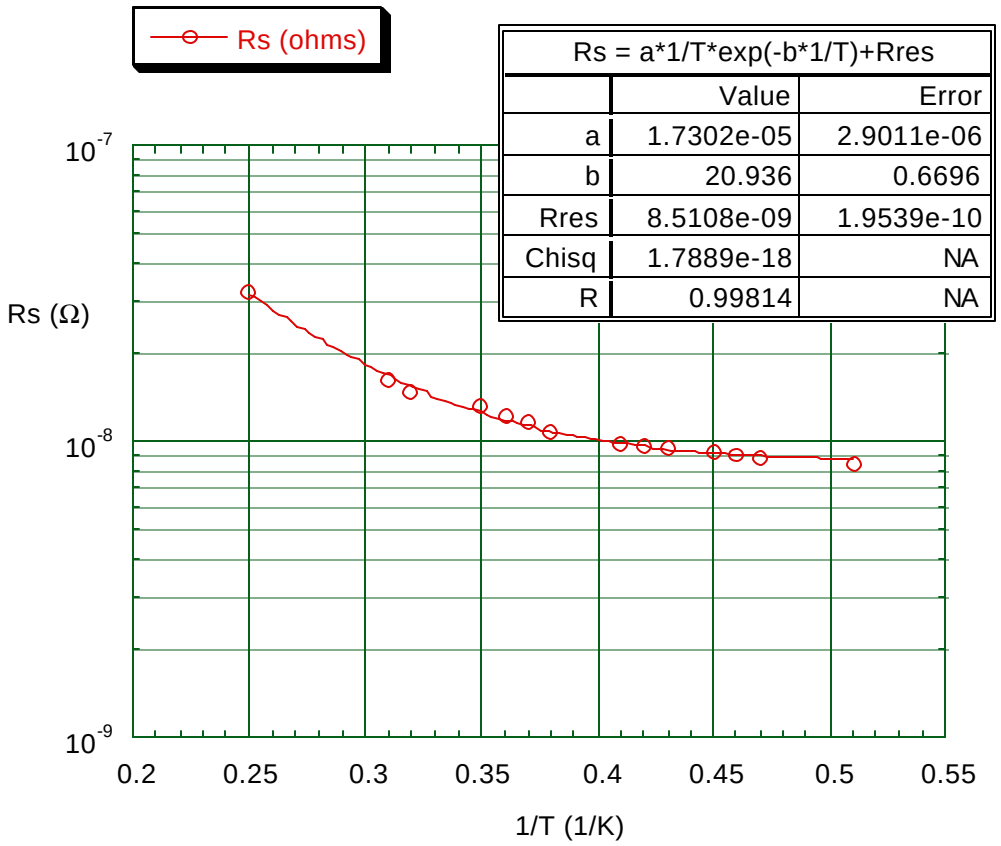

Fig. 17: Surface resistance as a function of 1/T, showing residual resistance of 8.5 nΩ.

3.4.2. X-ray

The data analyses of the PIN diodes are underway. We do not know if we could get any meaningful data since there was a lot of noise in the data. We hope we can report on the results of the data as soon as possible. As for the data on radiation monitor, the maximum radiation that we saw was about 83 mR/h, which was much lower compared to 700-MHz APT 5-cell elliptical cavities (>10 R/h).

Figure 18 shows the X-ray energy spectra obtained with NaI detector at 7.3 MeV/m at the first 2 K measurement. The maximum energy of the observed X-rays, ~980 KeV, corresponds to the maximum energy of the electrons that hit the cavity wall. A narrow peak around 80 KeV may be due to multipacting taking place somewhere in the cavity. It would be interesting to do some calculation on the electron impact energies at various areas in the cavity and identify where this X-ray came from.

Figure 19 shows the X-ray energy spectra during helium processing at 2 K. As one can see, the maximum energy increased significantly (~2.4 MeV). This is probably reflecting the energy of helium ions hitting the emission sources.

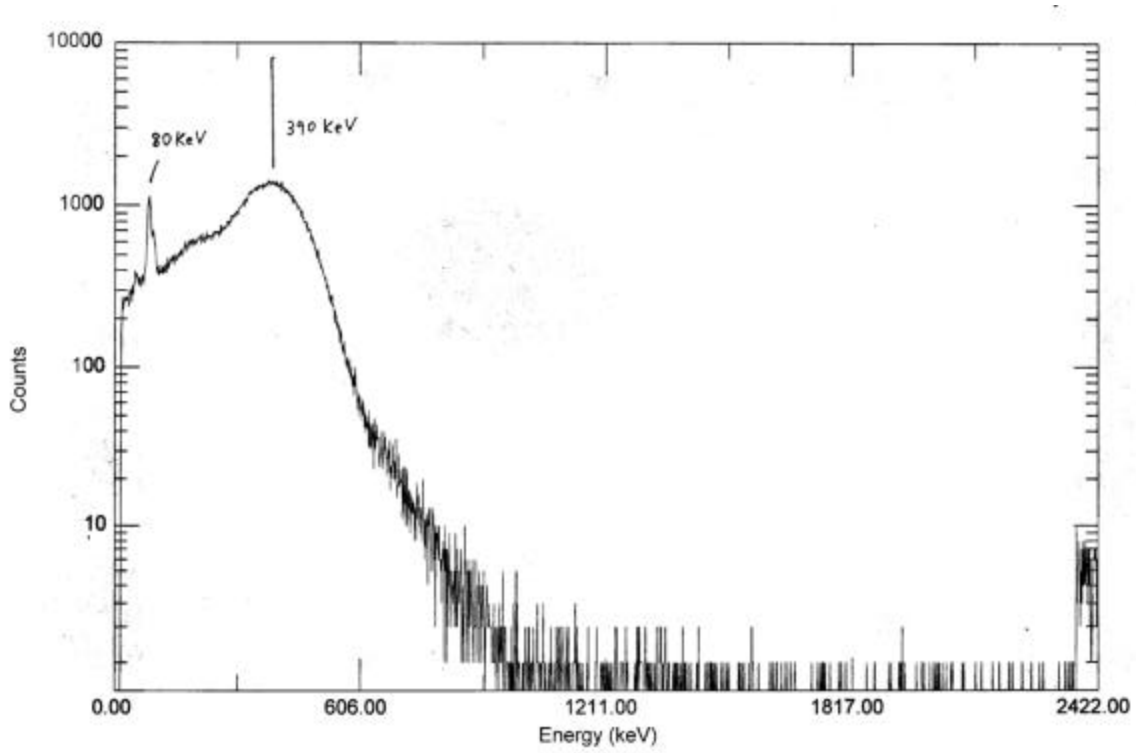

Fig. 18: X-ray energy spectra at 7.3 MeV/m in the first 2 K measurement.

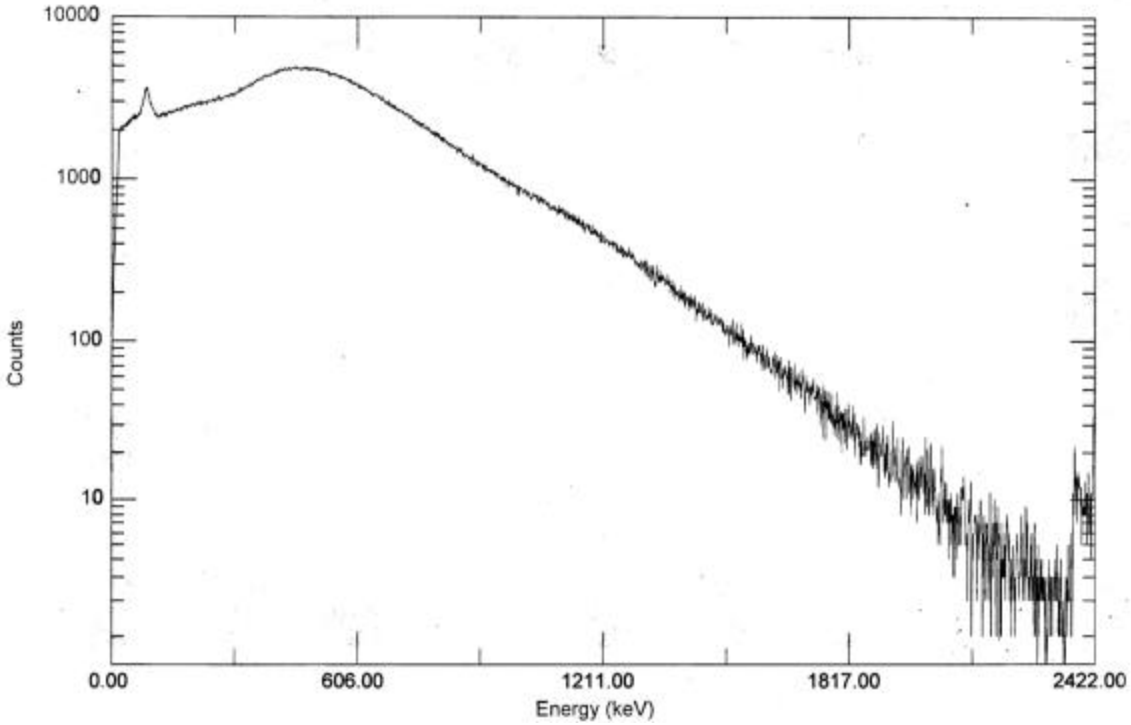

Fig. 19: Energy spectra during helium processing at 2 K.

4. Discussion

4.1. Q_0 and E_{acc}

Our result showed a factor of 4 higher Q_0 compared to that obtained at ANL at 4 K. Since BCS resistance should not be so different, the main reason for this seem to be the difference of residual resistance of the cavity surface. Since BCS resistance at 2.1 K is ~0.4 nΩ, the surface resistance is dominated by residual resistance. As shown in Section 3.3, the residual resistance in our test was 8.5 nΩ, whereas it is ~60 nΩ in the test at 2.1 K at ANL (Fig. 1). At the time of testing at ANL, there may have been insufficient cleaning after BCP. Recent results with β=0.4 cavity at ANL show better Q_0 with further high-pressure rinse [11].

4.2. Multipacting

We experienced some barriers at low field (E_{acc} < 2 MeV/m, ~3 MeV/m). It took us 10-20 minutes to process each time and there were a few times [12]. These may have been due to multipacting, although we are not sure about this since we were in the middle of tuning the RF system. Further tests will be needed to clarify what they were and where they came from. Practically, however, we will not have a problem at the operation gradient of 5 MeV/m unless we ramp up from 0 MeV/m or ramp down to lower fields during operation.

4.3. Field emission

Comparing Fig. 1 and Fig. 15, the field emission onset gradient increased from 3.5 MeV/m to 4.5 MeV/m with BCP of 100 microns alone, indicating that emitters have been partially removed with BCP. In our experience, though further BCP often improves the cavity performance, it rarely removes the emitters completely. We will have to develop a technique to localize and remove the emitters locally in the future to rescue the cavities that suffer severe field emission and cannot exceed the specification with further BCP.

4.4. Helium processing

As shown above, helium processing worked very well in this test. Unfortunately, however, helium processing does not always work like this. Especially, if the emitters are located at low electric field region, you cannot see much improvement or not at all. Also, it has been shown that the adsorbed gases on the emitters can re-activate the emitters and repetitive processing may be necessary to re-gain the effect of processing.
Anyway, establishing an automated helium processing technique will be worthwhile as one of the methods to improve the performance.

5. Summary

We demonstrated our capability of producing high Q_0 (>2 x 10^9 at 4 K, 3 times as high as ADTF specification) and high accelerating fields (>12 MeV/m, more than twice as high as ADTF specification) with the spoke cavity on loan from ANL. The highest electric field (12.5 MeV/m) corresponds to a

magnetic field of 1063 Gauss. This test showed that the type of cavity ANL designed, which is simpler and easier to fabricate compared to the one being designed at LANL, may be good enough for ADTF, although there is some room for improvement to facilitate easier cleaning, etc.

6. References

[1] T. Tajima, LANL Memorandum LANSCE-1:01-044, April 23, 2001.
[2] Scanned from the fax that K. Shepard of ANL sent to us on 2/27/01.
[3] Frank Krawczyk, LANL Memorandum LANSCE-1:01-014, Feb. 5, 2001.
[4] Calculated by Frank Krawczyk.
[5] This was borrowed from Philip Torrez of LANSCE-5.
[6] Though we were using 200 W amplifier, the maximum input power we were feeding for the amplifier was not saturated. We found this out the next day and could increase the output power of the amplifier.
[7] More automated system including automatic feeding is being planned.
[8] Unfortunately, the temperature sensor attached on the cavity was found to have fallen off during the test and we could not measure the exact cavity temperature. We estimated this temperature from our past warm-up data.
[9] H. Padamsee et al., *RF Superconductivity for Accelerators*, pg. 8, John Wiley & Sons, Inc. 1998.
[10] ibid [9] pg. 88.
[11] Mike Kelly of ANL, private communication.
[12] Since processing activities have not been logged much in detail, the exact number is unknown.
[13] Jens Knobloch, PhD thesis, CLNS THESIS 97-3, pp. 184-188, 1997.
[14] It is said that, when thermal breakdown or quench occurs, the speed at which the created normal conducting region disappears is as fast as a few to 10's of milliseconds. Compared to this speed, warm up and cool down manually will probably take on the order of seconds to minutes, which is referred as "slow" here.